Magnetic Hyperfine Structure of the $^3P_1$ and $^3P_2$ Metastable States of $Sn^{115,117,119}$†

W. J. CHILDS AND L. S. GOODMAN
Argonne National Laboratory, Argonne, Illinois
(Received 26 March 1964; revised manuscript received 26 August 1964)

The magnetic hfs of the metastable $^3P_1$ and $^3P_2$ states has been examined in the stable odd-A isotopes $Sn^{115,117,119}$. The interaction constant $a(^3P_1)$ is found to have the values +507.445(4), +552.608(4), and +578.296(4) Mc/sec in the isotopes Sn^{115}, Sn^{117}, and Sn^{119}, respectively. It is also found that $a(^3P_2)$ has the values −1113.770(4), −1212.956(3), and −1269.419(3) Mc/sec for the same isotopes. The results are compared with the theory. Values of the hyperfine anomalies are also given.

I. INTRODUCTION

THE magnetic field produced at the nucleus of an atom by the surrounding electronic configuration is not easy to calculate reliably. Although the field due to a pure Russell-Saunders level $^{2S+1}L_J$ may be calculated with fair accuracy, in practice the extent of any admixture is usually unknown. For the p^2 configuration of Sn the contribution of spin-orbit mixing within the configuration may easily be included, but admixtures due to interconfigurational interactions can also be large. In particular, polarization of the core by the outer electrons can contribute large fields at the nucleus. It is difficult to estimate the importance of such effects theoretically.

In the Sn atom, any internal magnetic field in the $^3P_1$ metastable state must arise from relativistic effects, from electron-core polarization, and from interconfigurational mixing. This field can be measured quantitatively.

Investigations[1] of the magnetic hyperfine structure (hfs) of the $^3P_1$ state of odd-A isotopes of Ge, which has the same electronic configuration as Sn (except for the principal quantum number), have shown that mixing effects are important and that the field at the nucleus is not zero. The present investigation shows that the effect is still more pronounced in Sn.

II. EXPERIMENTAL ARRANGEMENT

The atomic-beam magnetic-resonance apparatus used for the present investigation has been previously described.[2] The machine was operated with the conventional[3,4] "flop-in" arrangement produced by two 2-pole inhomogeneous magnetic fields. Atoms of the beam were detected by counting the ions produced by electron bombardment of the beam. The ions were mass analyzed to discriminate against the background not associated with the beam. The detected counts, after being scaled down to 40 000/sec or less, were fed to a bidirectional scaler (bds). The rf oscillator used to induce transitions was square-wave modulated at 10 cps. The same square wave was also used to gate the direction of the bds. On one half-cycle of the modulation signal, both signal and background counts were fed to the bds which was gated to scale forward; on the other half-cycle, only the background counts were fed to the bds, which was then gated to scale backwards. Thus, after any integral number of full cycles of the modulation signal, the number of counts on the bds was proportional to the signal strength. A preset scaler was used to select the number of cycles of the modulation signal during which each count was to be made. This number could be increased arbitrarily to improve the statistics.

It was also possible to square-wave modulate the entire atomic beam (instead of just the resonance signal) with a toothed-wheel mechanical chopper. This arrangement was extremely convenient for oven alignment. Observations of the transitions in the 0.35% abundant isotope Sn^{115} would not have been possible without the extreme sensitivity of the detector. Details of the detection system have been published.[2]

The Sn beam was produced by electron bombardment of the graphite oven containing the Sn. A single oven was used for all the measurements.

The 700–900-Mc/sec rf signal used to induce the $\Delta F=\pm 1$ transition in the $^3P_1$ metastable state of the stable odd-A Sn isotopes was produced by doubling the frequency output of a Solartron precision signal generator, Type DO 1001, and its range-extending synchronous amplifier. The frequency doubler, which utilized a step-recovery diode, was built by Micro-Beta Laboratories, Inc., Chicago. It operated with an efficiency of about 25%.

The 2800–3200-Mc/sec signal needed for the $\Delta F=\pm 1$ transition in the $^3P_2$ metastable state was produced by a phase-locked klystron. The locking was achieved with a Dymec oscillator synchronizer, Model 2650 A. The 37–42-Mc/sec output frequency of the Solartron precision signal generator was multiplied by 5 by a Solartron synchronous amplifier, Type 0 250. The synchro-

† Work performed under the auspices of the U. S. Atomic Energy Commission.
[1] W. J. Childs and L. S. Goodman, Phys. Rev. **131**, 245 (1963) and work in progress.
[2] W. J. Childs, L. S. Goodman, and D. von Ehrenstein, Phys. Rev. **132**, 2128 (1963).
[3] I. I. Rabi, J. R. Zacharias, S. Millman, and P. Kusch, Phys. Rev. **53**, 318 (1938); J. R. Zacharias, Phys. Rev. **61**, 270 (1942).
[4] W. J. Childs, L. S. Goodman, and L. J. Kieffer, Phys. Rev. **120**, 2138 (1960).

nizer locked the klystron to the sum of the 15th harmonic of the 185–210-Mc/sec signal and a separate variable 30-Mc/sec oscillator.

III. THEORY

The electronic ground-state configuration of the Sn atom is $5p^2$. The states arising from this configuration are, in order of increasing excitation energy, $^3P_0$ (the atomic ground state), $^3P_1$, $^3P_2$, $^1D_2$, and $^1S_0$. At the temperature of the atomic beam ($\sim$1400°C), the Boltzmann factors of the $^3P_1$ and $^3P_2$ states are large enough that transitions between hyperfine states in the 8%-abundant Sn^{117} and Sn^{119} can be seen without excessive difficulty. Similar measurements on the 0.35%-abundant Sn^{115} are, of course, about 20 times as difficult.

The values of the electronic g factors for the $J\neq 0$ states have previously been measured[5] with some precision. Table I summarizes this information.

TABLE I. Terms that arise from the p^2 electronic configuration of Sn I. The excitation energies[a] (in cm^{-1}) and Boltzmann factors are given. The previously measured electronic g factors[b] are given in column 4 for all states with $J\neq 0$.

Atomic state	Excitation energy (cm^{-1})	$e^{-E/kT}$	g_J
$^3P_0$	0.0	1.00	···
$^3P_1$	1691.8	0.22	1.50110(7)
$^3P_2$	3427.7	0.047	1.44878(9)
$^1D_2$	8613.0	0.0005	1.05230(8)
$^1S_0$	17162.6	very small	···

[a] C. E. Moore, Natl. Bur. Std. Circ. 467, Vol. III.
[b] See Ref. 5.

The isotopic abundances and basic nuclear ground-state properties of the three stable odd-A Sn isotopes $Sn^{115,117,119}$ are given in Table II. The nuclear ground

TABLE II. Abundance, nuclear spin I, and nuclear magnetic dipole moment[a] μ_I of the three stable odd-A Sn isotopes.

Isotope	Abundance (%)	I	μ_I (nm)
Sn^{115}	0.35	$\frac{1}{2}$	−0.917798(76)
Sn^{117}	7.61	$\frac{1}{2}$	−0.99990(19)
Sn^{119}	8.58	$\frac{1}{2}$	−1.04611(84)

[a] N. F. Ramsey, in *Handbook of Physics*, edited by E. U. Condon and H. Odishaw (McGraw-Hill Book Co., Inc., New York, 1958), pp. 9–69.

state is presumably due to the odd neutron in the $3s_{1/2}$ orbit. The magnetic dipole moments are seen to be the same to within less than 10%. The magnetic hyperfine interaction constants a can, within the uncertainties of hyperfine anomalies, be expected to be proportional to the dipole moments.

The Hamiltonian $\mathcal{H}$ for an individual Sn atom in an external magnetic field H is given[6] by

$$\mathcal{H}=ha\mathbf{I}\cdot\mathbf{J}+g_J\mu_0H(J_z+\gamma I_z), \quad (1)$$

where I and J are the nuclear spin and total electronic angular-momentum operators, respectively, and I_z and J_z are their projections on the field axis. The Bohr magneton is denoted by μ_0, and $\gamma=g_I/g_J$ is the ratio of the nuclear g factor g_I to the electronic g factor g_J. The g factors are defined by the conventional relations $\boldsymbol{\mu}_I=-g_I\mu_0\mathbf{I}$ and $\boldsymbol{\mu}_J=-g_J\mu_0\mathbf{J}$. The electric-quadrupole interaction is omitted because $I=\frac{1}{2}$.

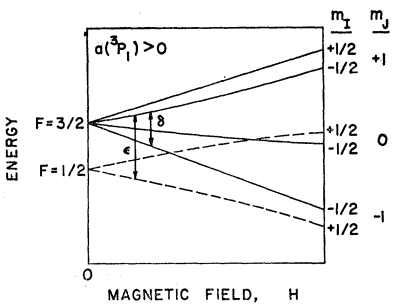

FIG. 1. Schematic hfs diagram for the stable odd-A Sn isotopes in the $^3P_1$ metastable atomic state. The magnetic-dipole hyperfine-interaction constant a has been taken to be positive, as determined experimentally. The two observed flop-in transitions are indicated.

The eigenvalues of this Hamiltonian are well known[1] and may be expressed as

$$E(J\pm\tfrac{1}{2},m_F)=\tfrac{1}{2}ah\{-\tfrac{1}{2}+2m_Fx \pm[(\tfrac{1}{2}(2J+1))^2-2m_F(1-\gamma)x+(1-\gamma)^2x^2]^{1/2}\}, \quad (2)$$

where m_F is the z projection of the total angular momentum of the atom (within the usual factor $\hbar$), h is Planck's constant, and x is the dimensionless parameter

$$x=(g_J\mu_0H/|a|h).$$

The hfs diagrams for the $^3P_1$ and $^3P_2$ metastable states of the $I=\frac{1}{2}$ Sn isotopes are shown in Figs. 1 and 2, respectively. These plots, which are just the schematic graphical representation of Eq. (2), indicate the observed flop-in transitions. If the double-quantum, flop-in transition in the state $F=I+J$ is denoted by a positive sign and the same transition in the state $F=|I-J|$ by a negative sign, then from Eq. (2) transitions α, β, and δ may be expressed as

$$\nu^{\pm}(J;\Delta F=0) =\nu_0(J)+\tfrac{1}{4}|a|\{[(\tfrac{1}{2}(2J+1))^2\mp(1-\gamma)x+(1-\gamma)^2x^2]^{1/2} -[(\tfrac{1}{2}(2J+1))^2\pm3(1-\gamma)x+(1-\gamma)^2x^2]^{1/2}\}, \quad (3)$$

where $\nu_0(J)$ denotes the transition frequency for the same metastable state in the even-even Sn isotopes, i.e.,

$$\nu_0(J)=g_J\mu_0H/h. \quad (4)$$

The transition ν^- is not observable in the $^3P_1$ state.

[5] W. J. Childs and L. S. Goodman, Phys. Rev. **134**, A66 (1964).

[6] N. F. Ramsey, *Molecular Beams* (Oxford University Press, New York, 1956), p. 272.

TABLE III. Transitions observed in Sn. The field-calibration data are given at the left, the odd-A Sn data at the right. The top section of the table deals with $\Delta F=0$ transitions, the bottom with $\Delta F=\pm 1$ transitions. The values of g_J and $|a|$ used in calculating the frequencies used in the last column are given in Tables I and IV, respectively. Where several isotopes are given in column 4, the resonances were unresolved.

Calibration resonance in even-even Sn isotopes			Resonances in odd-A Isotopes, $Sn^{115,117,119}$				
H (G)	Atomic state	Frequency (Mc/sec)	Mass number A	Atomic state	Transition observed	Observed frequency (Mc/sec)	$\nu_{obs}-\nu_{calc}$ (kc/sec)
1.000	$^3P_1$	2.102	115, 117, 119	$^3P_1$	δ	1.402(7)	0(7)
1.000	$^3P_1$	2.102	115, 117, 119	$^3P_2$	α	1.620(7)	+3(7)
5.002	$^3P_1$	10.510	115, 117, 119	$^3P_1$	δ	7.025(5)	+3(5)
5.002	$^3P_1$	10.510	115, 117, 119	$^3P_2$	α	8.116(5)	−2(5)
5.002	$^3P_1$	10.510	115, 117, 119	$^3P_2$	β	12.173(8)	+1(8)
15.008	$^3P_1$	31.533	115, 117, 119	$^3P_1$	δ	21.160(5)	−1(5)
15.008	$^3P_1$	31.533	115, 117, 119	$^3P_2$	α	24.358(7)	−6(7)
15.008	$^3P_1$	31.533	115, 117, 119	$^3P_2$	β	36.521(8)	−7(8)
40.018	$^3P_1$	84.080	117	$^3P_1$	δ	57.049(3)	−2(3)
40.018	$^3P_1$	84.080	119	$^3P_1$	δ	57.006(3)	−1(3)
40.018	$^3P_1$	84.080	115, 117, 119	$^3P_2$	α	65.015(5)	−5(5)
67.030	$^3P_1$	140.834	117	$^3P_2$	α	109.025(4)	+2(4)
67.030	$^3P_1$	140.834	119	$^3P_2$	α	109.013(4)	+2(4)
100.000	$^3P_1$	210.103	117	$^3P_1$	δ	146.462(5)	−4(5)
100.000	$^3P_1$	210.103	119	$^3P_1$	δ	146.166(5)	−5(5)
104.699	$^3P_1$	219.978	117	$^3P_2$	α	170.542(4)	−4(4)
104.699	$^3P_1$	219.978	119	$^3P_2$	α	170.514(5)	−1(5)
189.233	$^3P_2$	383.732	115	$^3P_2$	α	309.640(8)	+8(8)
189.233	$^3P_2$	383.732	117	$^3P_2$	α	309.400(6)	+9(6)
189.233	$^3P_2$	383.732	119	$^3P_2$	α	309.280(6)	+6(6)
1.000	$^3P_1$	2.101	115	$^3P_1$	ϵ	763.271(6)	
50.000	$^3P_1$	105.053	115	$^3P_1$	ϵ	872.650(7)	+8(7)
1.000	$^3P_1$	2.101	117	$^3P_1$	ϵ	831.015(6)	
1.000	$^3P_1$	2.101	119	$^3P_1$	ϵ	869.548(6)	
1.000	$^3P_1$	2.101	115	$^3P_2$	γ	2786.455(10)	
1.000	$^3P_1$	2.101	117	$^3P_2$	γ	3034.420(7)	
1.000	$^3P_1$	2.101	119	$^3P_2$	γ	3175.577(6)	

Similarly, the single-quantum $\Delta F=\pm 1$ flop-in transitions γ and ϵ may be expressed from Eq. (2) as

$$\nu(J;\Delta F=\pm 1)=\nu_0(J)+\tfrac{1}{2}|a|\{[(\tfrac{1}{2}(2J+1))^2-(1-\gamma)x+(1-\gamma)^2x^2]^{1/2}+[(\tfrac{1}{2}(2J+1))^2+(1-\gamma)x+(1-\gamma)^2x^2]^{1/2}\}. \quad (5)$$

All the flop-in observations of the present experiment are in quantitative agreement with Eqs. (3) and (5).

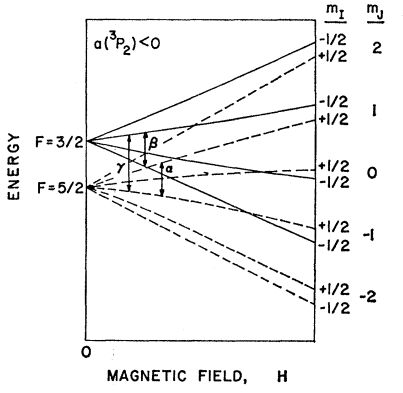

FIG. 2. Schematic hfs diagram for the stable odd-A Sn isotopes in the $^3P_2$ metastable atomic state. The magnetic-dipole hyperfine-interaction constant a has been taken to be negative, as determined experimentally. The three observed flop-in transitions are indicated.

In calculating the theoretical transition frequencies used in the last column of Table III, the values of g_J from Table I and the values of a from Table IV were used. The magnetic-field intensity for each measurement was determined by Eq. (4) from the observed resonance in the even-even Sn isotopes.

The treatment of Schwartz and Kopferman[7] enables one to calculate the values of a expected for the various metastable states of interest from the measured values of the nuclear magnetic dipole moments of the three isotopes $Sn^{115,117,119}$. Because the nuclear charge is rather large ($Z=50$), relativistic effects are important.

There is only one state with $J=1$ (the $^3P_1$ state) in the p^2 configuration, and it is most convenient to make the calculation in the j-j coupling scheme (the choice

TABLE IV. Values of, and ratios between, the a factors in the metastable $^3P_1$ and $^3P_2$ atomic states for the stable odd-A Sn isotopes. The signs of the a factors were measured absolutely.

Isotope	$a(^3P_1)$ (Mc/sec)	$a(^3P_2)$ (Mc/sec)	$a(^3P_2)/a(^3P_1)$
Sn^{115}	+507.445(4)	−1113.770(4)	−2.19 486(2)
Sn^{117}	+552.608(4)	−1212.956(3)	−2.19 497(2)
Sn^{119}	+578.296(4)	−1269.419(3)	−2.19 510(2)

[7] C. Schwartz, Phys. Rev. **97**, 380 (1955); H. Kopfermann, *Nuclear Moments* (Academic Press Inc., New York, 1958).

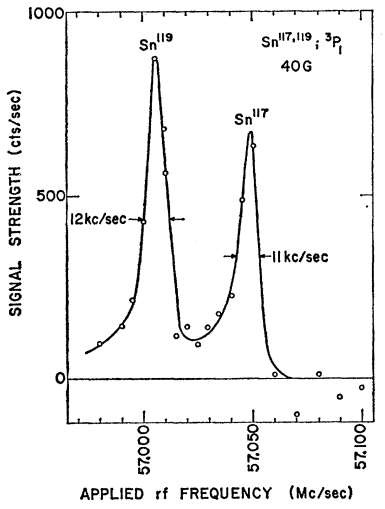

FIG. 3. Transition δ in Sn^{117} and Sn^{119} in the $^3P_1$ metastable state as observed at a field of 40 G. The splitting is due to the slight difference in the hyperfine interactions of the two isotopes.

of scheme used, of course, cannot affect the result). The state can be represented as $|\frac{1}{2},\frac{3}{2};1\rangle$. If relativistic effects are ignored, one finds $a(^3P_1)=0$. When, however, these effects are included, the calculated values are $a(|p_{1/2},p_{3/2};1\rangle)=192$, 209, and 219 Mc/sec, respectively, for the isotopes 115, 117, and 119.

For the $^3P_2$ state, one must make use of the intermediate-coupling composition of this state which has been determined by Childs and Goodman,[5] namely $|^3P_2'\rangle_{\text{int}}=-0.95451|^3P_2\rangle+0.29817|^1D_2\rangle$. Although not so dramatic, relativistic effects are important here too. The calculation then yields $a(^3P_2')_{\text{int}}=-1236$, -1347, and -1409 Mc/sec, respectively, for the isotopes 115, 117, and 119.

In Sec. V these numbers will be compared with the experimental results.

IV. EXPERIMENTAL PROCEDURE

A. Measurement of the Magnitudes of the a Factors

Operation of the atomic-beam machine was relatively straightforward for most of the experiment. On a typical run, additional Sn metal was added to the charge of the graphite oven, and the oven was heated to about 1400°C. Although the inhomogeneous "A" and "B" magnets were left on continuously, those atoms for which $M_J=0$ in the inhomogeneous fields were not deflected. The oven was aligned while detecting the undeflected beam with the universal detector. The modulation for the synchronous detection was produced by chopping the atomic beam mechanically at about 29 cps. The signal was displayed on a differential counting-rate meter which, of course, was not sensitive to the (unmodulated) background counts.

When the beam had been aligned, an obstacle wire was positioned to block the undeflected beam. The chopper was then turned off and the "C" field set by observing the resonance signal in the even-even Sn isotopes. This signal was very strong and could be observed easily on a dc counting-rate meter. Resonance s in the odd-A Sn isotopes were then examined point by point by introducing the square-wave-modulated r f signal of the appropriate frequency. The counts recorded on the bidirectional scaler for some fixed time were the measure of the signal strength.

Transition δ in the $^3P_1$ state was followed as the field was increased until the difference between the a factors of the isotopes produced a splitting into two components (one for each of the strong isotopes). Figure 3 shows this resolution in transition δ at 40 G. Good estimates of the a factors for Sn^{117} and Sn^{119} in the $^3P_1$ state were made from this observation. For both Sn^{117} and Sn^{119} the transition was further followed, as indicated in Table III, to give still better determinations for the $^3P_1$ state of Sn^{117} and Sn^{119}.

Transition ϵ was then observed for both Sn^{117} and Sn^{119} at 1 G. No transition had yet been observed in the weak isotope Sn^{115} but the ratios $\mu_I(Sn^{115})/\mu_I(Sn^{117})$ and $\mu_I(Sn^{115})/\mu_I(Sn^{119})$ were known[8] accurately from NMR work. These ratios and the present values of $|a(Sn^{117};{}^3P_1)|$ and $|a(Sn^{119};{}^3P_1)|$ were used to predict the value of $|a(Sn^{115};{}^3P_1)|$ on the assumption of zero hyperfine anomaly. A search around the predicted frequency at 1 G quickly showed the Sn^{115} transition ϵ as shown in Fig. 4, thus establishing the small size of the hyperfine anomaly. This transition was also observed at 50 G as a further check on its identity.

Transitions α and β in the $^3P_2$ state were also followed to higher fields. The appearance of transition α in all three isotopes at 189.233 G is shown in Fig. 5. The resonance in Sn^{115} was weak and difficult to observe. The same transition in the other two isotopes was very strong; in order to ensure a narrow line width, the rf power was reduced until the peak height dropped about a factor of 4. This accounts for the fact that the Sn^{117} and Sn^{119} peaks appear only about 5 times as strong as the Sn^{115} instead of 20 times as expected from the relative isotopic abundances. It can also be noted that the

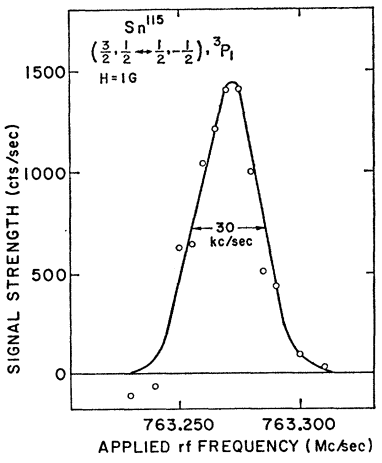

FIG. 4. Transition ϵ in the $^3P_1$ metastable state of Sn^{115} as observed at 1G.

[8] W. G. Proctor, Phys. Rev. **79**, 35 (1950).

Sn^{115} resonance is wider than the other two because of the higher rf power used.

The mass numbers of the three resonances were identified by changing the ion-acceleration voltage by the appropriate mass ratios and observing the change in the relative intensities. The resolution of the mass spectrometer (as used in the present experiment) was such that all three masses could be observed simultaneously, although the one for which the spectrometer was optimized was relatively favored. The very small hyperfine anomalies observed (discussed below) constitute convincing support of the mass identifications.

Once the data shown in Fig. 5 had been taken, the values of a could be reliably calculated for all three isotopes in the $^3P_2$ metastable state. Searches at 1 G then revealed transition γ in all three isotopes. Figure 6 shows the appearance of transition γ in Sn^{117} at 1 G.

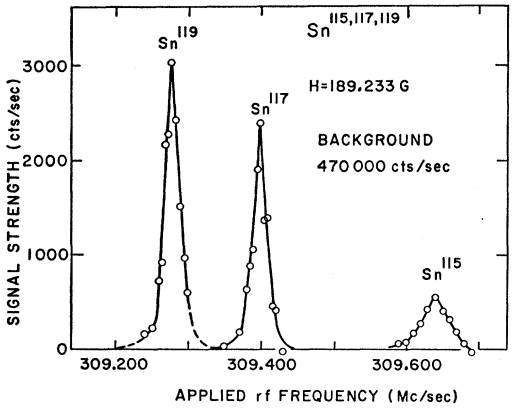

FIG. 5. Transition α in the $^3P_2$ metastable state of $Sn^{115,117,119}$ as observed at 189.233 G. The failure of the observed relative intensities to correspond to the known isotopic abundances is due primarily to the use of reduced rf power for observation of the transition in the two strong isotopes Sn^{117} and Sn^{119}. This was done (at the expense of counting rate) to ensure a narrow linewidth. The observed width of the Sn^{115} transition, which was observed at a greater rf power level, is greater than for the other two isotopes.

B. Measurement of the Signs of the a Factors

The experimental arrangement used for the determination of the signs of the a factors is shown schematically in Fig. 7. The technique has been successfully used[4,9] before. The only changes from the first part of the experiment are the addition of a second rf loop in the homogeneous "C" field and the replacement of the centrally positioned obstacle wire by a half-plane obstacle. The obstacle is positioned in such a way that it intercepts all the atoms of the beam that would have been intercepted by the wire, and in addition, blocks all atoms that would have passed on one side of the wire. It is necessary to know which side of the apparatus has been made opaque and also to know the direction of the field gradients in the inhomogeneous fields.

[9] J. G. King and V. Jaccarino, Phys. Rev. 94, 1610 (1954).

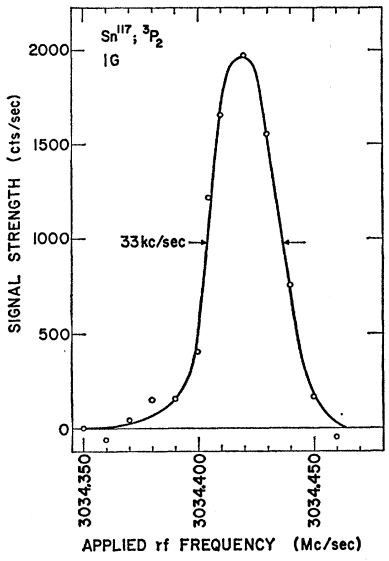

FIG. 6. Transition γ in the $^3P_2$ metastable state of Sn^{117} as observed at 1 G.

The value of m_J in the first inhomogeneous ("A") magnet will be denoted by $m_J(A)$. The present arrangement allows only those atoms for which $m_J(A)$ is negative to travel past the half-plane obstacle in the second inhomogeneous ("B") magnet. Whether or not these atoms with $m_J(A)<0$ reach the detector depends on their deflection in the "B" magnet, which in turn depends on which transitions they have undergone in the "C" field.

Figure 8 shows the magnetic-field dependence of the $F=\frac{3}{2}$-level for the odd-A, $I=\frac{1}{2}$ Sn isotopes in the $^3P_1$ metastable state for both possible signs of the hyperfine interaction constant a. At 20 G, the resonance frequencies of the double-quantum flop-in transition δ and the single-quantum flop-out transitions η and ζ differ from each other by many linewidths and are thus fully resolvable.

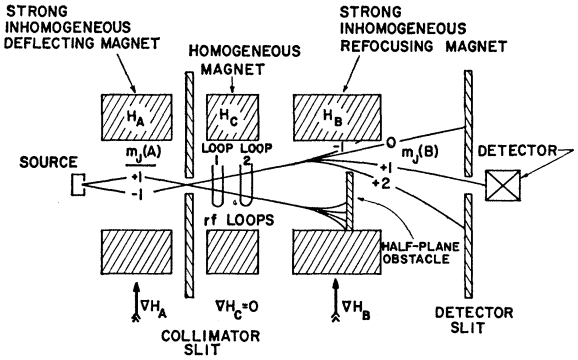

FIG. 7. Schematic view of the experimental arrangement as used for the measurement of the signs of the a factors. With the indicated arrangement of the field gradients and half-plane obstacle, only atoms for which $m_J=-1$ in the strong inhomogeneous "A" magnet need be considered. The two rf loops are used to induce two different transitions in the same atom as it passes through the homogeneous "C" field. The technique is described in the text.

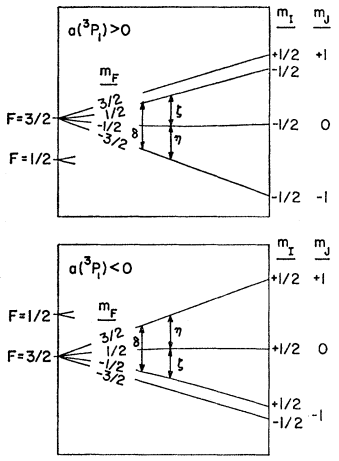

FIG. 8. Schematic hfs diagram of the $F=\frac{3}{2}$ component of the $^3P_1$ state, drawn for both signs of the hyperfine-interaction constant a. Those transitions that are useful for determination of the sign of the interaction are indicated.

Atoms of the beam for which $m_J(A)=0, +1$ need not be considered since they cannot pass the half-plane obstacle. If ν_λ denotes the resonance frequency for transition λ, then atoms for which $m_J(A)=-1$ may undergo transition δ if ν_δ is applied to, say, loop 1. The case $a(^3P_1)>0$ will be considered first. If the number of atoms flopped in by the application of ν_δ on loop 1 is noted, and then ν_ζ is applied to loop 2, some of those atoms that would have reached the detector are flopped out and the detected flop-in signal is reduced. In other words, those atoms for which $m_J(B)=+1$ have been been flopped to $m_J(B)=0$ and consequently cannot be detected. If $a(^3P_1)<0$, application of ν_ζ on loop 2 will not affect the intensity of the flop-in signal. The trajectories for the various possibilities are shown schematically in Fig. 7.

If the signals ν_δ and ν_ζ are applied in the reverse order, the situation is different. Application of ν_δ on loop 2 will, of course, still produce the flop-in signal. If $a(^3P_1)>0$, application of ν_ζ on loop 1 can only lead to transitions between states for which $m_J(A)=0, +1$ and thus cannot alter the flop-in signal which is induced at loop 2. (The only observable effect of the flop-in signal is to flop atoms from $m_J(A)=-1$ to $m_J(B)=+1$.) If $a(^3P_1)<0$, application of ν_δ to loop 2 again induces the flop-in transition $m_J(A)=-1$ to $m_J(B)=+1$. Application of ν_ζ to loop 1 can, however, reduce the population of atoms that have both $m_J(A)=-1$ and $m_F=-\frac{1}{2}$ and thus could undergo the subsequent flop-in transition δ.

Thus, if ν_δ is applied continuously to loop 1, and ν_ζ is applied to loop 2, a reduction of the flop-in signal is to be expected only if $a(^3P_1)>0$. If ν_δ is applied continuously to loop 2 and ν_ζ to loop 1, then the reduction will occur only if $a(^3P_1)<0$. Figure 9 shows the results of the experiment. The resonant dip in the flop-in signal δ is centered around ν_ζ when ν_δ is applied to loop 1 and ν_ζ to loop 2. This establishes that $a(^3P_1)>0$.

The slight dip in the lower curve of Fig. 9 is believed to be due to imperfect localization of the rf fields (which were only about 2 cm apart). Inhomogeneities in the "C" field (so that not all regions of the field in which transitions occur are at exactly 20 G) could also introduce irregularities. The result of the experiment is considered unambiguous because of the deep and resonant nature of the observed dip.

The field at which the experiment was performed (20 G) was not high enough to resolve the different Sn isotopes. Thus, if the a factor of the strong isotopes $Sn^{117,119}$ in the $^3P_1$ state were of opposite sign, interpretation of the results would be complex. Convincing evidence that the a factor does not change in sign (for a given metastable level) in going from Sn^{115} to Sn^{117} and Sn^{119} is that the measured sign of μ_I is the same for all three isotopes.[8]

It may be noted that transition η could have been used in place of ζ. If it had, the interpretation would be the reverse of that given. The resonance frequencies ν_ζ and ν_η are sufficiently different (more than 10 linewidths at 20 G) that identification of the flop-out transition as ζ is unambiguous.

Analysis of the corresponding experiment in the $^3P_2$ state is entirely similar to that given above for the $^3P_1$ state. The $F=\frac{3}{2}$ level was selected, and the field $H=39$ G was chosen to assure good separation of the resonance frequencies for transitions β, θ, ι, and κ (Fig. 10). Transition κ is analogous to ζ, and ι is analogous to η; transition θ has the same effect as ι and occurs because atoms flopping out of the state $m_J(B)=+1$ can now go to $m_J=+2$ as well as to 0. For the experiment, transition θ was selected for the flop-out signal. Figure 11 shows the resonant dip in the flopped-in signal strength as a function of ν_θ. Transition θ was induced in loop 2 for the data of the upper curve, and in loop 1 for those of the lower curve. Because transition θ is equivalent in effect to ι and hence to η, it is opposite to ζ and the inferred sign of a is therefore opposite. It is

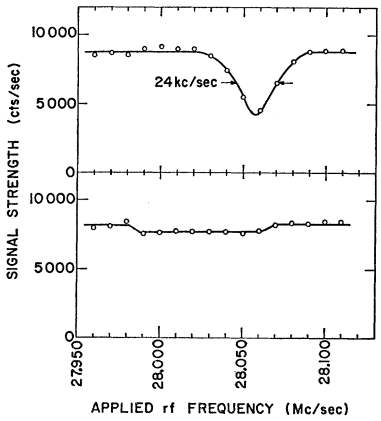

FIG. 9. Changes in the flop-in signal strength of transition δ in the $^3P_1$ metastable state as the frequency of the applied flop-out signal ζ is varied in the appropriate range. The upper curve results when the flop-in signal is fed to the first loop and the flop-out signal to the second. The lower pattern results when the sequence of the loops is reversed. The measurements were made at 20 G.

thus clear that $a(^3P_2)<0$. As in the $^3P_1$ state, no differentiation between the isotopes $Sn^{115,117,119}$ was made in determining the sign of $a(^3P_2)$.

V. RESULTS AND CONCLUSIONS

The single-quantum $\Delta F=\pm 1$ transitions ϵ (in the $^3P_1$ metastable state) and γ (in the $^3P_2$ state) were observed at 1 G for each of the three isotopes $Sn^{115,117,119}$. Magnitudes of the magnetic-dipole hyperfine-interaction constants a were deduced from these results with the aid of Eq. (5). The signs of the interaction constants were then measured as described above. The results are summarized in Table IV. The ratio of the a factor in the $^3P_2$ state to that in the $^3P_1$ state is also given for each isotope. This ratio is seen to vary slowly but definitely as the mass number is increased.

The theoretical predictions for the a factors (with interconfiguration interactions ignored) have been given above. For purposes of discussion, we will consider only the Sn^{117} isotope. The discussion describes the situation of the a factors for the other two isotopes equally well.

The difference $(a_{\text{expt}}-a_{\text{calc}})$ for the $^3P_1$ state is $\delta(^3P_1)=553-209=344$ Mc/sec. For the $^3P_2'$ state, we have $\delta(^3P_2')=-1213-(-1347)=134$ Mc/sec.

One must consider the differences $\delta(^3P_1)$ and $\delta(^3P_2')$ in the light of atomic-core polarization by the outer p electrons. If relativistic effects and intermediate coupling could be ignored, the contributions to the two δ's from core polarization should be equal. With these effects included the two contributions would no longer be expected to be equal, but their ratio would not be very different from one. Unfortunately, the calculations of the a factors are based on assumptions which cast doubt on their precision and thus make quantitative considerations of the core polarization to be of dubious reliability. (1) Interconfiguration mixing was ignored. (2) The value of $a_p=\epsilon\langle|r^{-3}|\rangle$ was derived from the spectroscopic fine-structure splitting, and was used for both $p_{1/2}$ and $p_{3/2}$ electrons along with the appropriate $F(r)$ and $G(r)$ integrals from Kopfermann. (3) A "reasonable" value of an effective nuclear charge has to be chosen. In the present calculations the value $Z'=Z-4$ was assumed. Because of these various uncertainties, the calculations of the a factors are probably no more precise than $\pm 15\%$. One can adjust a_p within this range so that two δ's can indeed be brought to have the correct ratio for the intermediate coupling, relativistic calculation. Until the calculation can be made on a better physical model, however, such adjustments are without too much meaning.

With these limitations one can only say that at the nucleus the magnetic field due to core polarization is in the same direction as that due to the outer electrons for the $^3P_1$ state, and in the opposite direction for the $^3P_2$ state; and that the δ's can be accounted for in terms of atomic-core polarization within the limits of theoretical prediction.

Since the ratios of the nuclear magnetic dipole moments for the different isotopes have been measured[8]

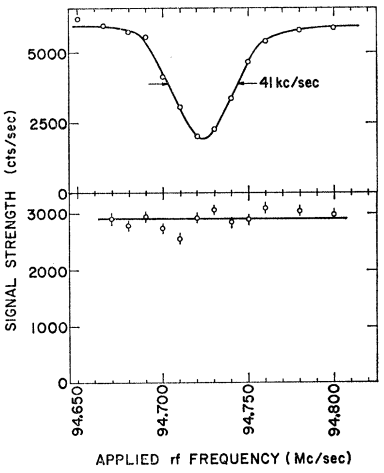

FIG. 11. Changes in the flop-in signal strength of transition β in the $^3P_2$ metastable state as the frequency of the applied flop-out signal θ is varied in the appropriate range. The upper curve results when the flop-in signal is fed to the first loop and the flop-out signal to the second. The lower pattern results when the sequence of the loops is reversed. The measurements were made at 39 G.

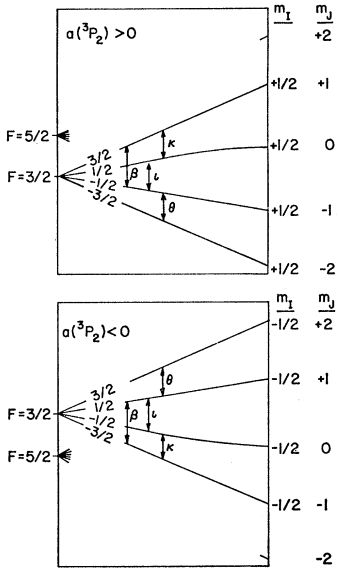

FIG. 10. Schematic hfs diagram of the $F=\frac{3}{2}$ component of the $^3P_2$ state, drawn for both signs of the hyperfine-interaction constant a. Those transitions that are useful for determination of the sign of the interaction are indicated.

TABLE V. Measured values of the hyperfine anomaly in two metastable atomic states. The uncertainties originate in the measurement[a] of the ratios of the nuclear magnetic dipole moments.

Isotope pair	Metastable atomic state $^3P_1$	$^3P_2$
Sn^{115}–Sn^{117}	+0.00037(10)	+0.00032(10)
Sn^{117}–Sn^{119}	+0.00001(10)	−0.00005(10)

[a] See Ref. 8.

to 1 part in 10,[4] the hyperfine anomalies (as defined on p. 280 of Ref.6) can be calculated. The results are given in Table V. The precision is, at present, limited by the uncertainties given for the ratios of the dipole moments.

The magnetic field produced at the Sn nucleus by the electronic configuration can be obtained from the relation[2]

$$H_J=-\frac{haIJ}{\mu_I}. \tag{6}$$

From Tables II and IV and Eq. (6), the internal fields are found to be

$$H(^3P_1)=+0.3626\times10^6\ \mathrm{G},$$
$$H(^3P_2)=-1.592\times10^6\ \mathrm{G},$$

to within about 0.1%.

ACKNOWLEDGMENTS

The authors would like to thank B. Budick for a helpful private communication. They are extremely grateful to Brian Wybourne for extensive hfs calculations and numerous helpful discussions.

PHYSICAL REVIEW VOLUME 137, NUMBER 1A 4 JANUARY 1965

Approximate Methods for Obtaining Radial Distribution Functions of Fluids*

D. D. CARLEY AND F. LADO
Department of Physics, University of Florida, Gainesville, Florida
(Received 14 August 1964)

Two integral equations are proposed whose solutions approximate the radial distribution function of classical fluids whose single-component particles interact with pairwise radial forces. Solutions to these equations are obtained for several temperature and density conditions for particles interacting with potentials corresponding to the Lennard-Jones, the hard-sphere, and the Gaussian models. When Monte Carlo results are used as a standard, these new equations provide answers which often show improvement over the answers obtained by the Percus-Yevick or convolution-hypernetted-chain equations.

I. INTRODUCTION

THE theory of fluids in thermodynamic equilibrium has undergone considerable progress in recent years as a result of studies of the radial distribution function g[1]. Although several new methods have been advanced for computing g, the convolution-hypernetted-chain[2] (CHNC) and the Percus-Yevick[3] (PY) equations have received the greatest attention. A large number of solutions have now been obtained for these equations over a wide range of temperature and density conditions for several forms of the pair potential function[4] and these results indicate that the PY and CHNC equations provide considerable improvement over previous methods. However, neither the PY nor the CHNC equation has obtained a clear advantage over the other for all potentials under varying temperature and density conditions.

The PY and CHNC equations may be looked upon as a partial summation of terms[5] (from all orders of density) of the density expansion for g. The CHNC summation includes all the terms summed by PY plus an additional infinite set. The remarkable success of the PY equation, in spite of its summation of fewer terms, suggests that there is often better cancellation among the terms omitted than in the CHNC equation. The techniques of summation of certain terms from the density expansion, as exemplified by the CHNC and PY equations, suggests two possible procedures for obtaining better distribution functions: (1) to systematically include more terms in the summation or (2) to eliminate more terms or to weight certain ones differently to obtain better cancellation among the terms

* This research was supported in part by the National Science Foundation and the National Aeronautics and Space Administration.

[1] For a general discussion of the radial distribution function, its relationship to various thermodynamic quantities, and its role in the theory of fluids, see, J. O. Hirschfelder, C. F. Curtiss, and R. B. Bird, *Molecular Theory of Gases and Liquids* (John Wiley & Sons, Inc., New York, 1954).

[2] E. Meeron, J. Math. Phys. **1**, 192 (1960); T. Morita, Progr. Theoret. Phys. (Kyoto) **23**, 385 (1960); J. M. J. Van Leeuwen, J. Groeneveld, and J. DeBoer, Physica **25**, 792 (1959); M. S. Green, Technical Report, Hughes Aircraft Corporation (unpublished).

[3] J. K. Percus and G. J. Yevick, Phys. Rev. **110**, 1 (1958); J. K. Percus, Phys. Rev. Letters **8**, 462 (1962).

[4] A. A. Broyles, J. Chem. Phys. **33**, 456 (1960); **34**, 359, 1068 (1961); **35**, 493 (1961); A. A. Broyles, S. U. Chung, and H. L. Sahlin, *ibid.* **37**, 2462 (1962); A. A. Khan, Phys. Rev. **134**, A367 (1964); D. D. Carley, *ibid.* **131**, 1406 (1963); D. D. Carley, *ibid.* **136**, A127 (1964); M. Klein, J. Chem. Phys. **39**, 1388 (1963); M. Klein and M. S. Green, *ibid.* **39**, 1367 (1963); M. Klein, Phys. Fluids **7**, 391 (1963); M. S. Wertheim, Phys. Rev. Letters **10**, 321 (1963).

[5] The original derivation as published by Percus and Yevick employed collective coordinates. G. Stell studied the equation from the summation point of view. G. Stell, Physica **29**, 517 (1963). See also Khan, Ref. 4.